Journal of Energy Storage 19 (2018) 73–87

Contents lists available at ScienceDirect

Journal of Energy Storage

journal homepage: www.elsevier.com/locate/est

Revisiting the dual extended Kalman filter for battery state-of-charge and state-of-health estimation: A use-case life cycle analysis

Nikolaos Wassiliadis[a,*], Jörn Adermann[a], Alexander Frericks[b,1], Mikhail Pak[b], Christoph Reiter[a], Boris Lohmann[b], Markus Lienkamp[a]

[a] Chair of Automotive Technology, Department of Mechanical Engineering, Technical University of Munich (TUM), Germany
[b] Chair of Automatic Control, Department of Mechanical Engineering, Technical University of Munich (TUM), Germany

ARTICLE INFO

Keywords:
Dual extended Kalman filter
Battery state estimation
State-of-charge estimation
State-of-health estimation
Battery management systems

ABSTRACT

One of the most discussed topics in battery research is the state-of-charge (SOC) and state-of-health (SOH) determination of traction batteries. Unfortunately, neither is directly measurable and both must be derived from sensor signals using model-based algorithms. These signals can be noisy and erroneous, leading to an inaccurate estimate and, hence, to a limitation of usable battery capacity. A popular approach tackling these difficulties is the dual extended Kalman filter (DEKF). It consists of two extended Kalman filters (EKFs), that synchronously estimate both the battery states and parameters. An analysis of the reliability of the DEKF estimation against realistically fading battery parameters is still a widely discussed subject. This work investigates the DEKF performance from a high-level perspective, involving different load dynamics and SOH stages. A numerical optimization-based approach for the crucial filter parameterization is employed. We show that the DEKF partly improves the accuracy of the SOC estimation compared to the simple EKF over battery lifetime within the operational limits of an automotive application. However, capacity and internal resistance estimation becomes unreliable and partly diverges from the reference under constant and realistic load scenarios coupled with advanced degradation. As a consequence, a downstream use of both parameters in a SOC or SOH estimation is hampered over the battery lifetime. Extensions are needed to improve reliability and enable employment in real-world applications.

1. Introduction

Since battery electric vehicles (BEVs) have been seen as a solution to both local and global air pollution, research has increasingly focused on the competitiveness with conventional internal combustion powertrain solutions [1]. Still, the range and price are significant hurdles associated with raising customer acceptance of BEV [2]. Both directly depend on a full exploitation of the available resources of the vehicle.

For a given and applied system, effective utilization of drivetrain components mainly depends on precise determination of the present condition of the energy storage, which can be determined, *inter alia*, through precise knowledge of the battery's crucial quantities state-of-charge (SOC) and state-of-health (SOH) [3]. If there is no accurate information on the SOC and SOH available, safety margins have to be reserved, so that the operational limits are not exceeded during operation [4]. This leads either to a limited range specification of the vehicle, since capacity is not used to its full potential, or to a battery oversizing leading to additional weight. Therefore, a precise estimation of SOC and SOH is of the highest importance in order to entirely utilize the available capacity. With an accurate SOC and SOH estimation, not only can the battery capacity be fully exploited, but also cost-saving potential can be addressed by downsizing the battery system. In addition, both quantities are unitless and have to be further processed for a physical interpretation as a range by the user, which is why the accuracy of both quantities is also user-critical during operation.

Unfortunately, SOC cannot be measured directly and has to be derived from common measurement quantities, such as current, temperature and voltage [5]. The SOC is commonly defined as the current integral normalized to the actual capacity C_p, measured at 20 °C ambient temperature with a full CCCV discharge cycle between the operating voltage limits. 0% SOC hereby corresponds to a fully discharged and 100% SOC to a fully charged battery. The continuous-time dependence of the terminal current i to the SOC of the battery is defined as

* Corresponding author.
E-mail address: wassiliadis@ftm.mw.tum.de (N. Wassiliadis).
[1] Current correspondence: Chair of Autonomous Systems Technology, University of the Bundeswehr München, Germany.

https://doi.org/10.1016/j.est.2018.07.006
Received 26 March 2018; Received in revised form 14 June 2018; Accepted 6 July 2018
Available online 23 July 2018
2352-152X/

Table 1
Review of various DEKF applications for battery state and parameter estimation.

Year	Author	Model	Initialization	Deviation/extension	Analyzed estimate
2004	Plett [18–20]	Several models	n/s	None	States/Parameter
2007	Urbain et al. [41]	R_0 model	Tuned	None	States/Parameter
2008	Lee et al. [42]	1-RC model	n/s	Adaptive noise	States/Parameter
2009	Rubagotti et al. [43]	2-RC model	n/s	Multi-timescale setup	States/Parameter
2012	Hu et al. [44]	ESC model [18]	n/s	Multi-timescale setup	States/Parameter
2013	Kim and Cho [45]	1-RC model	n/s	Machine-learning extension	States/Parameter
2013	Mastali et al. [46]	Hysteresis model [18]	Measured	None	States
2013	Dragicevic et al. [47]	R_0 model	n/s	None	States/Parameter
2014	Walder et al. [48]	1-RC model	Measured	None	States/Parameter
2014	Xiong et al. [49]	1-RC model	n/s	Multi-timescale setup	States/Parameter
2014	Campestrini et al. [50]	1-RC model	n/s	None	States/Parameter
2016	Campestrini et al. [51]	2-RC model	Tuned	None	States
2016	Nejad et al. [52]	2-RC model	Tuned	Decoupled capacity estimation	States/Parameter
2018	Li et al. [53]	2-RC model	Tuned	Multi-timescale setup	States/Parameter

n/s: not specified.

$$\mathrm{SOC} = \mathrm{SOC}_0 + \frac{1}{C_p}\int_{t_0}^{t_1} i(t)\mathrm{d}t \tag{1}$$

where the remaining quantity SOC_0 is the initial SOC.

However, measurements for this definition are typically corrupted by noise and other measurement errors [6,5]. Moreover, biases in low-cost sensors or external disturbances can lead to further divergence from the true value and therefore distort the SOC prediction [7,8]. Since the definition from Eq. (1) demands an initial value SOC_0, which cannot be predicted accurately per definition [5,6], biases can also occur here. In addition, the usable capacity C_p is a variant parameter that fades with time and has to be updated precisely in order to avoid offsets and drifts in the estimate.

The usable capacity is also a key figure for the determination of battery SOH, commonly defined as

$$\mathrm{SOH} = \frac{C_p}{C_0} \tag{2}$$

where C_0 represents the rated capacity specified per design and measured under the aforementioned conditions prior to operation. Complex degradation processes within the battery cell lead to a fading capacity and a rising ohmic resistance, mainly induced by a loss of active material of the electrodes and a loss of lithium inventory, e.g. due to growth of the solid electrolyte interphase (SEI), decomposition reactions or irreversible lithium plating [9–12]. Those processes occur during the cycling [13] as well as during storage [14] of the battery. Both, a fading capacity and rising ohmic resistance, drag down the general performance of the battery. Precise information about internal resistance and capacity is important to assess whether the battery can still serve within the operational specifications. Here, the same barriers as for the SOC estimation occur.

1.1. Literature review

In the past, many advanced methods for SOC and SOH estimation were presented to overcome the aforementioned hurdles, involving specific advantages and disadvantages.

For SOC estimation, machine learning approaches such as fuzzy logic [15], artificial neural networks [16] or SVM [17] were used. These methods can yield high estimation accuracies but are compromised of high experimental effort to gather training data and still suffer under the weaknesses of an open-loop prediction. Therefore, also many closed-loop approaches were presented, involving electrical models such as the extended Kalman filter (EKF) [18–22], sigma point Kalman filter and its applications as an unscented Kalman filter (UKF) or central difference Kalman filter [23–27], and particle filter (PF) [28,29] – with rising implementation and calculation complexity and rather moderate improvement in accuracy [5,8,30]. Also, extended numerical approaches such as moving horizon estimation (MHE) [31], sliding-mode observer (SMO) [32], partial differential equation estimation techniques [33], H-infinity observer [34], nonlinear geometric observer [35], and Luenberger-type observer [36] were studied involving a similar trade-off between accuracy and complexity.

For SOH estimation, many of the aforementioned methods were coupled or extended to concurrently estimate SOC and SOH with the specific inherited benefits and drawbacks of the involved methods. E.g. the EKF was applied for both estimation tasks in a fourth-order joint estimation with promising results but only offline operation because of stability and computational complexity [37]. For an online implementation, also the triple combination of a linear Kalman Filter, a UKF and a SVM was broadly analyzed [38], with the necessity for training data. Dual SMO [39], dual PF [40] and dual MHE [31] were applied as well, involving high computational effort of the battery management system (BMS).

In order to estimate SOC and SOH synchronously online without intensive upfront effort and to meet the rigorous real-time requirement on a vehicular BMS, many authors applied the popular dual extended Kalman filter (DEKF) approach to the underlying estimation problem. An overview can be found in Table 1.

Plett [18–20] introduced the DEKF for estimating capacity and resistance in a single use-case scenario. Despite promising convergence results in a long-term estimation under an erroneous initialization, the instantaneous capacity estimation is presented under a correct initialization only; without offsets due to an incorrect initial estimate. Also, the effect on SOC estimation is not presented. Urbain et al. [41] adapted the DEKF method for two use-case scenarios in a real-time environment, namely a photovoltaic and a hybrid electric vehicle (HEV) application. While the resistance estimation shows convergence to a static value in the dynamic HEV scenario, the capacity estimation is characterized by noise under constant load in the photovoltaic scenario. Unfortunately, covariance initialization is not specified. Lee et al. [42] extended the DEKF method by employing a rule-based algorithm extension involving adaptive noise covariances for capacity estimation. Under specific use-case scenarios and different erroneous initializations, a parameter estimation error range below 5% can be achieved. However, convergence speed of the DEKF estimation is low. Rubagotti et al. [43] proposed a multi-timescale strategy for estimating the capacity of a lead-acid battery without specifying the used noise covariances. An equal multi-timescale strategy is employed by Hu et al. [44] for capacity estimation of lithium-ion batteries (LIB) in order to improve the stability of the capacity estimate. Kim and Cho [45] proposed a combination of a DEKF with a machine-learning approach to concurrently estimate SOC and capacity of a battery. In the work of Mastali et al. [46], DEKF is used to improve the estimation accuracy of battery SOC. In contrast to previously discussed studies, noise covariances are

gathered by measuring the noise of the sensors. Dragicevic et al. [47] used a simple R_0-model of the battery to estimate the internal resistance over a week of experimental data with good convergence of the estimate. Walder et al. [48] showed that SOC and model parameter can be estimated for the Artemis driving cycle at a specific SOH with promising results in SOC estimation with an error below 1.5%. Xiong et al. [49] provided an extensive analysis of the multi-timescale DEKF approach for capacity estimation under several stages of aging. Campestrini et al. [50] extended the analysis to different temperature levels between 5 and 35 °C, with an overall SOC estimation error below 1.5%. It is stated, that noise covariances were tuned manually according to the particular temperature scenario. In another publication, Campestrini et al. [51] compared the DEKF to various Kalman filter-based algorithms in an extensive analysis with special detail to cross influences of the employed battery model and different temperature stages. The authors concluded that the DEKF improves the SOC estimation performance if covariances are tuned optimally. Nejad et al. [52] analyzed the DEKF performance on-chip with a decoupled capacity estimation extension and a single-load scenario. Here, covariances are initialized by arbitrarily specified values. Li et al. [53] provided a detailed analysis of dual estimation frameworks involving the DEKF for capacity estimation. The results showed that the DEKF outperforms the other methods, namely the PF and the least squares approach, in longterm stability. However, if the DEKF is initialized incorrectly by a wrong guess for battery capacity, the convergence behavior of the DEKF needs hours to converge to a close neighborhood of the true value. If the ohmic resistance of the battery is estimated as well, SOC and capacity estimation can be improved.

1.2. Contributions

Despite intensive research on the DEKF method as previously mentioned, the need for further investigations of the reliability of DEKF is still present [54]. Several studies point out that different load dynamics, the choice of a specific battery model and an increasing model error due to degradation are important side-effects, that deteriorate the DEKF accuracy and thus reliability during operation. In order to assess the effect of load dynamics, mostly standardized or synthetic load scenarios are applied. However, the battery sees rather dynamic and unpredictable load profiles in real automotive use-case scenarios. Furthermore, while the convergence behavior of the parameter estimates is analyzed in the context of converging to a true reference value, the cross-influence on SOC estimation is not intensively discussed - which is particularly important if battery capacity is incorrectly initialized with a static over-estimated value during vehicle lifetime. Here, long convergence times jeopardize the SOC estimation stability. Moreover, besides the use of many different battery cell models, there is still no consensus about how to properly initialize and tune the DEKF, which is crucial for the filter performance and should be put into practice with care.

Consequently, the main objectives of this contribution is to answer the question if, and if yes, how reliably and robustly the DEKF can estimate SOC and SOH under battery degradation from a high-level, automotive use-case perspective. To cover a wide range of possible operating states, that is constant and dynamic driving scenarios over battery lifetime, different load dynamics and aging stages are applied. Special detail is given to an applicable, careful and simple determination and transparent specification of the initial filter parameters (state and parameter covariances, noise covariances) in an automotive application. Since the parameter estimation influences not only the SOH determination, but also the SOC estimation, the DEKF is initialized in a way that estimation convergence is numerically optimal within a given cycle. Cross-influences between state and parameter estimation under the given initialization are investigated.

1.3. Paper organization

The remainder of this paper is structured as follows: Section 2 introduces the applied battery model and the DEKF in detail to get a common understanding of the theoretical background. Subsequently, the approach of the underlying assessment is exhibited in Section 3. The results are then presented and discussed in Section 4. Finally, Section 5 summarizes the strengths and weaknesses of the DEKF method for SOC and SOH estimation and provides recommendations for further research on that field.

2. Theoretical background

For a comprehensive understanding of the scope of the analysis that is carried out, the used models and estimation algorithms are presented in the subsequent sections.

2.1. Equivalent circuit model

The most important part of any estimation problem is a carefully crafted model that imitates the behavior of the battery. An exact model replica of LIB is almost impossible, due to the complex behavior in operation and the limited calculation capability of commonly employed BMS [55]. In order to encounter this problem with a satisfying accuracy, many researchers employ ECMs to the underlying problem [56]. A widely used model for LIB hereby consists of a capacitance C_p, a series resistance R_0 and two RC elements with the resistances and capacitances R_1, C_1, R_2, C_2; as illustrated in Fig. 1. The capacitance C_p models the usable battery capacity, whose voltage slope is represented by the open circuit voltage (OCV) U_{OCV}. Serial resistance R_0 represents the ohmic voltage drop of the contact resistance and inner ohmic resistances of the processes within the battery cell. The first and the second RC elements model the voltage drop under dynamic load and thus the occurring cell-internal polarization and diffusion phenomena, respectively [57,58]. The only directly measurable quantities of the system are the terminal current i as the controllable input and the terminal voltage U as the measurable output.

The applied ECM can be described as a third-order nonlinear state-space system

$$x_{k+1} = f(x_k, u_k) \tag{3a}$$

$$y_k = g(x_k, u_k) \tag{3b}$$

where the state vector x_k describes the current, non-measurable state of the system. u_k describes the terminal current as measured input and y_k the terminal voltage as measured output. The state space transition is described by $f(x_k, u_k)$ and the measurement equation by $g(x_k, u_k)$. Applying the corresponding physical relationships in discrete time, one obtains

$$x_k = \begin{bmatrix} \mathrm{SOC} \\ U_{\mathrm{RC1}} \\ U_{\mathrm{RC2}} \end{bmatrix}, \quad u_k = i_k, \quad y_k = U_k \tag{4a}$$

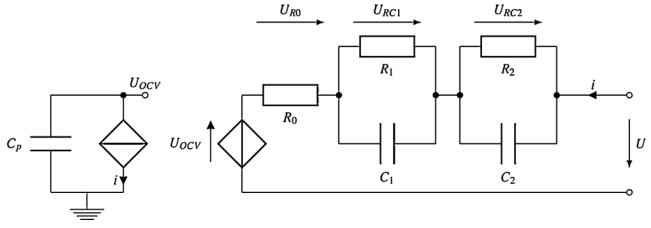

Fig. 1. Equivalent circuit model (ECM) with the open-circuit voltage U_{OCV}, the ohmic resistance R_0 and the two RC-elements RC_1, RC_2.

$$f\left(\begin{bmatrix} x_k \\ u_k \end{bmatrix}\right) = \begin{bmatrix} \mathrm{SOC} + \frac{\mathrm{d}t}{C_p} i_k \\ U_{\mathrm{RC1}} e^{-\frac{\mathrm{d}t}{R_1 C_1}} + \left(1 - e^{-\frac{\mathrm{d}t}{R_1 C_1}}\right) R_1 i_k \\ U_{\mathrm{RC2}} e^{-\frac{\mathrm{d}t}{R_2 C_2}} + \left(1 - e^{-\frac{\mathrm{d}t}{R_2 C_2}}\right) R_2 i_k \end{bmatrix} \tag{4b}$$

$$g(x_k, u_k) = U_{\mathrm{OCV}}(\mathrm{SOC}) + U_{\mathrm{RC1}} + U_{\mathrm{RC2}} + R_0 i_k \tag{4c}$$

It should be noted that the state transition equation $f(\cdot)$ is linear, which can be seen if the vector is decomposed with respect to x_k and u_k. A nonlinearity occurs only in the SOC–OCV correlation within the measurement equation $g(\cdot)$.

2.2. Extended Kalman filter

The introduced cell model and the state-space equations from Eq. (3) provide a physical relation between the input, state and output quantities. With this feature at hand, we can employ an observer algorithm to obtain a good estimate of the states of the system while measuring the input and output of the cell model. For the sake of simplicity, we only partly highlight specific points and avoid a detailed presentation of the EKF algorithm. The reader is referred to extensive literature within that field [59,18–20], which is where the following excerpt is taken from with slight index modifications.

Plett [18] linked the Kalman observer design to the battery SOC estimation by using the modified state space

$$x_{k+1} = f(x_k, u_k) + q_k^x \tag{5a}$$

$$y_k = g(x_k, u_k) + r_k^x \tag{5b}$$

with the added stochastic noise terms q_k^x and r_k^x (zero-mean white Gaussian), described by the noise covariance matrices Q^x and R^x, respectively. The applied noise covariance matrices allow the filter to adjust the states according to the confidence in the estimate, which is a weighted balance between the measurement and the model prediction. As shown in Section 2.1, the nonlinearity of the state space requires an extension of the original linear Kalman observer algorithm. Thereupon, Plett [18] presented the EKF (Fig. 2) which linearizes the nonlinear system equations at each sample point. For the battery model introduced in Section 2.1, this results in the Jacobian matrices

$$\hat{A}_k = \frac{\partial f(\cdot)}{\partial \hat{x}_k^+} = \begin{bmatrix} 1 & 0 & 0 \\ 0 & e^{-\frac{\mathrm{d}t}{R_1 C_1}} & 0 \\ 0 & 0 & e^{-\frac{\mathrm{d}t}{R_2 C_2}} \end{bmatrix} \tag{6a}$$

$$\hat{C}_k = \frac{\partial g(\cdot)}{\partial \hat{x}_{k+1}^-} = \begin{bmatrix} \frac{\partial U_{\mathrm{OCV}}}{\partial \mathrm{SOC}} \Big|_{\hat{x}_{k+1}^-} & 1 & 1 \end{bmatrix} \tag{6b}$$

and enables a fair state estimation if the BMS sample intervals are small.

If the state space model is parameterized accurately with respect to the monitored battery cell and the noise covariances are initially set properly, the filter proves to be stable, convergent and robust against erroneous starting values while assuring a high accuracy of the estimate [18] as long as the battery is new and matches the model well.

However, not all model parameters are time-invariant [18,60,61]. The internal resistance increases and the usable capacity decreases simultaneously due to aging processes over the lifetime of the cell, commonly known as battery degradation [9–12]. As an appropriate threshold for vehicular applications, many authors define the end-of-life (EOL) of an automotive battery at $0.8 \cdot C_p$ [5,6,11,38]. Moreover, the SOC-OCV correlation changes over time [61]. Consequently, the time-invariant and therefore erroneous modeling of the aforementioned parameters generates a steadily increasing model error within the observer, which jeopardizes the filter's stability and convergence [61,60,62].

One possible countermeasure can be a time-variant parameterization of the fading parameter by using experimental techniques and aging models [11]. However, this approach is expensive due to laborious and time-consuming experiments, such as accelerated aging tests [11], or simply not applicable for online estimation because high-precision testing equipment is not available in the vehicle [63,64]. Furthermore, aging models place high demands on BMS resources, which hampers a direct implementation. Another option lies in initially increasing the process noise covariance in the equations affected by degradation in order to cover the increasing model error [61]. Unfortunately, again laborious aging experiments are necessary to adjust the noise covariances appropriately, since an incorrect parameterization, that is an under- or overestimate, leads to a steadily divergent or too-noisy filter behavior, respectively [65]. In addition, the important information on the SOH is neglected, since physical parameters are not estimated. An adaptive determination of the noise covariances could also stabilize the filter [66], but without providing the aforementioned important physical information on the parameter and thus SOH.

2.3. Dual extended Kalman filter

In order to maintain observer stability over the vehicle lifetime and to avoid laborious test or resource deployment, Plett [20] extends the framework by 1 s EKF (Fig. 3). The first observer (EKF^x) estimates the fast-varying state (x_k) and the second observer EKF^θ synchronously estimates the slow-varying parameter (θ_k) of the plant model within the first EKF. State EKF is run with priority, so that the remaining voltage error can be used by the second EKF to adjust the parameters accordingly. Both observers exchange the information about the estimates recursively at each sample point.

The dynamics of the first filter, EKF^x, are defined by Eq. (3). Furthermore, the dynamics of the second filter for the parameter estimation task are defined by

$$\theta_{k+1} = \theta_k + q_k^\theta \tag{7a}$$

$$y_k = g(x_k, u_k, \theta_k) + r_k^\theta \tag{7b}$$

where q_k^θ and r_k^θ are parameter process and measurement noise with the noise covariances matrices Q^θ and R^θ, respectively. The parameter

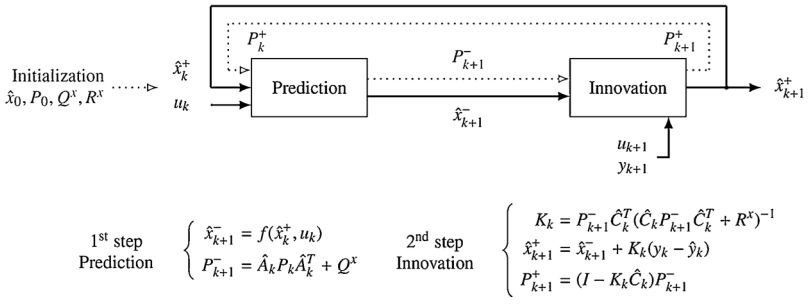

Fig. 2. Schematic scheme of the nonlinear EKF with the corresponding calculation sequence for the prediction and innovation step (from top to bottom each) [18,59].

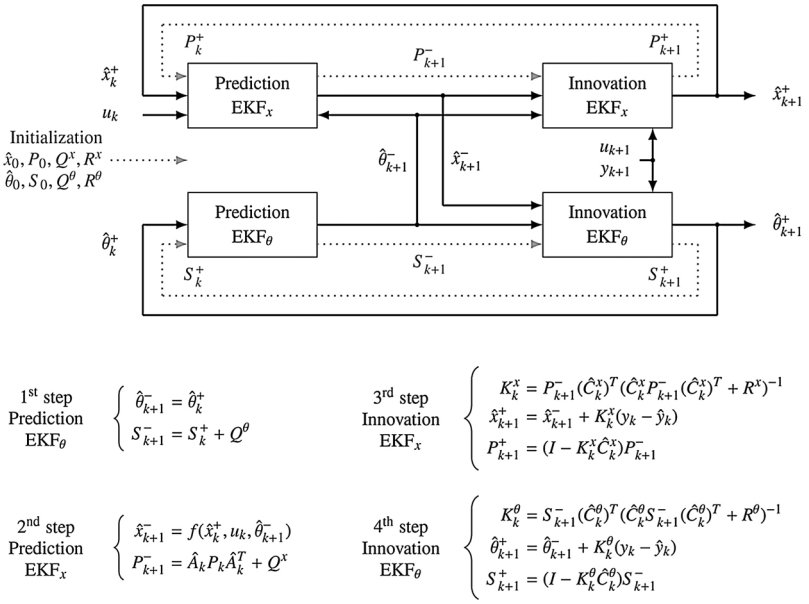

Fig. 3. Schematic scheme for the nonlinear DEKF with the corresponding calculation sequences for the prediction and innovation step (from top to bottom each) [20,59].

vector θ_k is modeled as constant and disrupted by the process noise only. An adaption to the true value is only possible by applying the unknown noise terms within the DEKF algorithm.

With this general formulation at hand, we still need to define which parameters we want to estimate. Since the focus is on testing the reliability of the DEKF under applied circumstances and thus without excessive usage of resources, we only take the strongly varying parameters C_p and R_0 into account. The first does not only strongly vary over the battery lifetime, it is also mandatory for tracking the SOH according to the definition from Eq. (2). Hence, the investigated parameter vector is defined as

$$\theta = \begin{bmatrix} C_p \\ R_0 \end{bmatrix}. \tag{8}$$

As seen for the state estimation, a linearization has to be performed for the parameter estimation as well. Since the innovation step of the EKF$^\theta$ is run subsequent to the innovation step of the EKF^x and the values of $\hat{x}_k$ have to be considered too, the Jacobian $\hat{C}^\theta_k$ is more laborious to obtain. With the general total derivative formulation

$$\hat{C}^\theta_k = \left.\frac{\mathrm{d}g(\hat{x}^-_{k+1}, u_{k+1}, \theta)}{\mathrm{d}\theta}\right|_{\theta=\hat{\theta}^-_{k+1}} \tag{9a}$$

$$\frac{\mathrm{d}g(\hat{x}^-_{k+1}, u_{k+1}, \theta)}{\mathrm{d}\theta} = \frac{\partial g(\hat{x}^-_{k+1}, u_{k+1}, \theta)}{\partial \theta} + \frac{\partial g(\hat{x}^-_{k+1}, u_{k+1}, \theta)}{\partial \hat{x}^-_{k+1}} \frac{\mathrm{d}\hat{x}^-_{k+1}}{\mathrm{d}\theta} \tag{9b}$$

$$\frac{\mathrm{d}\hat{x}^-_{k+1}}{\mathrm{d}\theta} = \frac{\partial f(\hat{x}^+_k, u_k, \theta)}{\partial \theta} + \frac{\partial f(\hat{x}^+_k, u_k, \theta)}{\partial \hat{x}^+_k} \frac{\mathrm{d}\hat{x}^+_k}{\mathrm{d}\theta} \tag{9c}$$

$$\frac{\mathrm{d}\hat{x}^+_k}{\mathrm{d}\theta} = \underbrace{\frac{\mathrm{d}\hat{x}^-_k}{\mathrm{d}\theta}}_{=0,\ k=0} - K^x_k \underbrace{\frac{\mathrm{d}g(\hat{x}^-_k, u_k, \theta)}{\mathrm{d}\theta}}_{=0,\ k=0} \tag{9d}$$

where the *a priori* unknown terms of Eq. (9d) are initialized with zero and the remaining terms from Eqs. (9b and 9c) implemented according to

$$\frac{\partial g(\hat{x}^-_{k+1}, u_{k+1}, \theta)}{\partial \theta} = [0 \quad i_{k+1}] \tag{10a}$$

$$\frac{\partial g(\hat{x}^-_{k+1}, u_{k+1}, \theta)}{\partial \hat{x}^-_{k+1}} = \left[\left.\frac{\partial U_{\mathrm{OCV}}}{\partial \mathrm{SOC}}\right|_{\hat{x}^-_{k+1}} \quad 1 \quad 1\right] \tag{10b}$$

$$\frac{\partial f(\hat{x}^+_k, u_k, \theta)}{\partial \theta} = \begin{bmatrix} -\frac{\mathrm{d}t}{C_p^2} i_k & 0 \\ 0 & 0 \\ 0 & 0 \end{bmatrix} \tag{10c}$$

$$\frac{\partial f(\hat{x}^+_k, u_k, \theta)}{\partial \hat{x}^+_k} = \begin{bmatrix} 1 & 0 & 0 \\ 0 & e^{-\frac{\mathrm{d}t}{R_1 C_1}} & 0 \\ 0 & 0 & e^{-\frac{\mathrm{d}t}{R_2 C_2}} \end{bmatrix} \tag{10d}$$

with respect to the introduced battery model from Section 2.1 and the aforementioned parameter vector θ at the operating point $\hat{\theta}^-_{k+1}$, the total derivative is fully solved.

2.4. Observability

As mentioned previously, SOC and SOH cannot be measured directly and must be derived from available sensor signals with the aid of a system model. However, this indirect determination, which is based on observation, is not always possible, especially if the given system is nonlinear.

The simplest example of a non-observable system is one with a non-injective nonlinearity in the measurement equation, e.g. $\dot{x} = 0$, $y = \sin x$. Although straightforward for the linear time-invariant system class, observability analysis remains a challenging issue for nonlinear problems [67,68]. A proper nonlinear observability analysis can be performed in some simple cases, but in the practical case, one often resorts to investigating proxy properties such as parameter sensitivity [69], or one relies on simulation-based investigations.

Observability of the EKF for SOC estimation has already been verified [70]. The results have shown, that unobservable conditions do not occur within the operating range of the battery. In our application case for the concurrent DEKF estimation of SOC and SOH, a theoretical observability analysis is infeasible: the observability investigation of the highly nonlinear joint state-parameter problem is not applicable to the employed dual state-parameter observer algorithm. Hence, we performed multiple simulations (Section 4) and compared the estimates with the known reference (ground truth) SOC and SOH value. Although this approach cannot prove observability, it can be used to show non- or weak observability of some parameters for the given estimation setup.

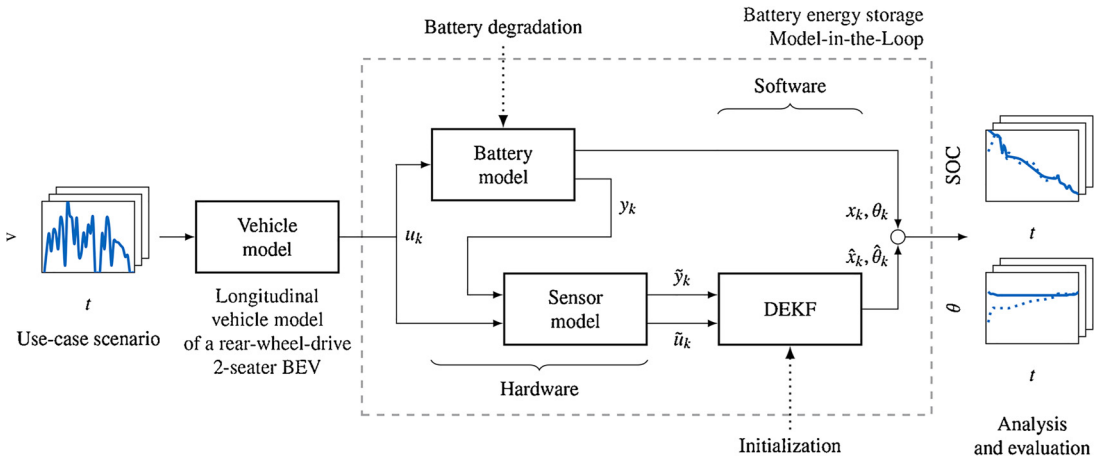

Fig. 4. Model-in-the-Loop framework for a holistic assessment of the overall DEKF performance under SOH, load and initial dataset variation.

3. Approach

The use-case analysis of the DEKF performance is carried out by using a MIL approach, since parameter modifications can be set effectively and long-term experiments are avoided. The general framework is illustrated in Fig. 4 and consists of the core energy storage model and a corresponding in- and output.

Several use-case scenarios can be specified as velocity data points and transformed to a load profile by employing a longitudinal vehicle model of a rear-wheel-drive 2-seater BEV. The resulting power profiles are then applied to the energy storage model as an input and are numerically scaled down to a single battery cell. Within the energy storage model, the physical battery cell that shall be measured is also modeled in order to easily and replicably apply different SOH stages to the filter without laborious experiments. Before the battery signal enters the DEKF algorithm, noise and analog/digital quantization errors are artificially added within a sensor submodel. The simulated noisy "measurement" is then processed by the DEKF with a given initialization dataset. In the final step, the estimated states and parameters can be compared to the reference states from the battery model. The vehicle and the sensor model are derived from a BEV available on-site.

In the following sections, the defined use-case scenarios, the approach to model the battery degradation and the used filter implementation and initialization are presented and explained in detail.

3.1. Use-case scenarios

As stated in Section 2, different dynamics have a crucial impact on the DEKF estimation behavior. The dynamics' influence is analyzed by applying three different velocity profiles to the vehicle model in order to map different dynamics, that is

(1) low dynamics: derived from a synthetic velocity profile with a velocity plateau at 50 km/h and an acceleration and deacceleration phase;
(2) high dynamics: derived from the synthetic Artemis urban cycle with a transient slope; and
(3) real dynamics: derived from a real-world test drive with the available on-site battery-electric vehicle [71];

resulting in three different power profiles for the energy storage (Fig. 5). All cycles are repeated until the SOC reaches 10%.

3.2. Degradation modeling

The second variable, the SOH of the estimated battery, is phenomenologically modeled and realized by using different parameter sets for

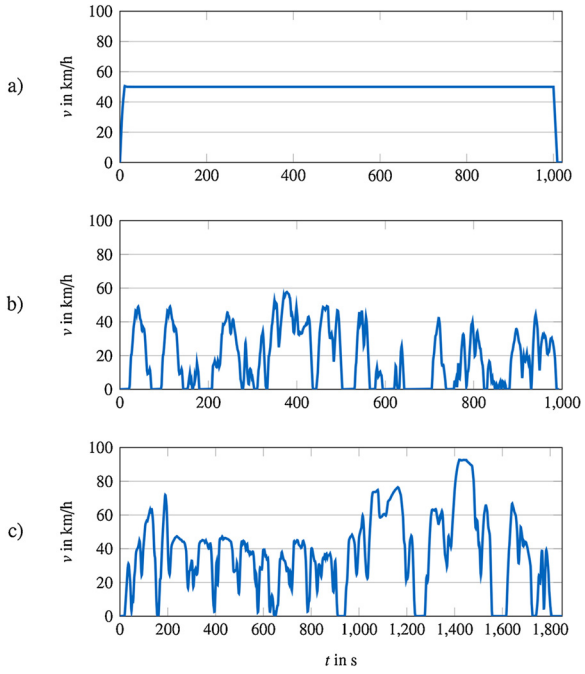

Fig. 5. Overview of the applied use-case scenarios: (a) Low dynamics scenario with a constant velocity plateau at 50 km/h, (b) High dynamics scenario according to the ARTEMIS urban, (c) Real dynamics scenario logged with the on-site available battery electric test vehicle.

the introduced MIL battery model. Therefore, five 18,650 cells from the same batch with a nominal capacity of 2.9 Ah are used, four cells thereof are artificially cycled with a synthetic profile and characterized at different stages of the aging process, defined by the loss of usable capacity compared to the capacity of a new cell as stated in Eq. (2). Electrochemical impedance spectroscopy (EIS) and parameter fitting in the frequency domain is used to parameterize the ECM. For parameter determination, pseudo-potentiostatic EIS measurements are performed at 100, 90, 75, 50, 25, 10 and 0% SOC in the frequency range of 5 kHz to 10 mHz. All SOC levels are reached by constant current (CC) discharge with the respective charge amount. The actual cell capacity is determined beforehand by CC-CV charge and subsequent CC-CV discharge within the voltage limits of 4.2 and 2.5 V, respectively.

All model parameters are provided in Fig. 6. One SOH parameter set is gathered close to the new cell, two are gathered close to the automotive EOL criterion and the last is taken from a sophisticated SOH stage at 49%, far beyond the recommended automotive EOL, to

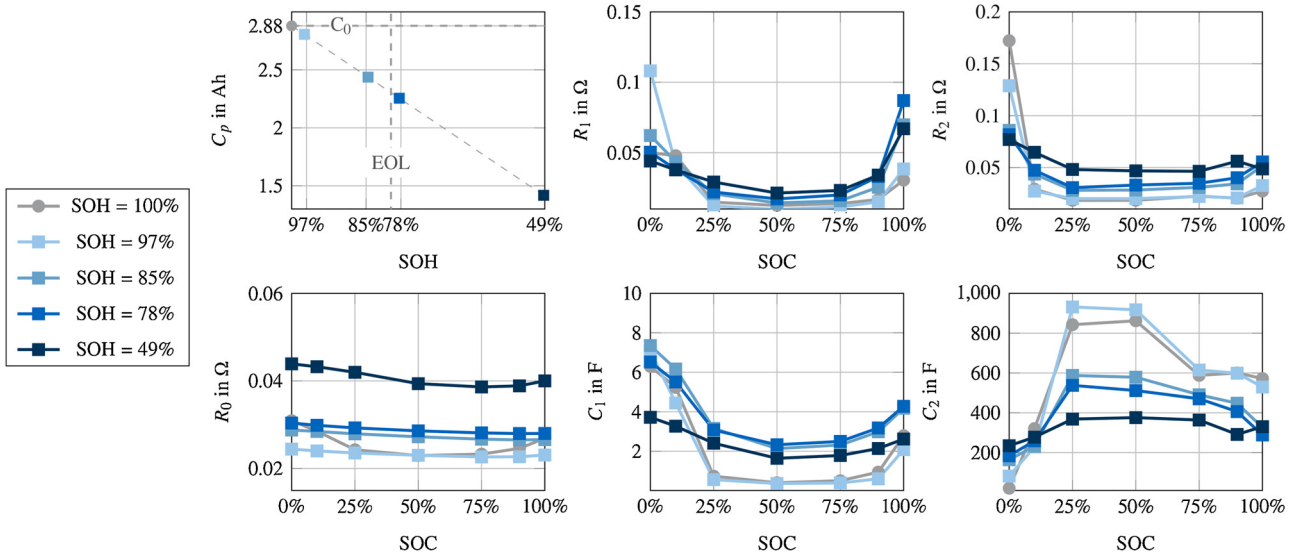

Fig. 6. Battery degradation parameter sets at different SOH stages fitted to a 2-RC element ECM battery model with electrochemical impedance spectroscopy with the capacity C_p and the ohmic resistance R_0 in the first column, the elements R_1 and C_1 of the first RC-element in the second column and the elements R_2 and C_2 of the second RC-element in the third column.

illustrate an automotive afterlife or another energy demanding application. Per definition, a linear capacity loss can be seen over SOH. As expected, also an overall increase in ohmic resistance can be observed during aging with a steady distribution over SOC. It should be noted that between 100% SOH and 97% SOH, the ohmic resistance slightly decreases, which can be traced back to inaccuracies of the numerical fitting algorithm of the impedance response in the frequency domain, since the model cannot entirely map the impedance behavior of the real cell (see Section 3.4 for the chances and limits of this approach). Besides, also a great variation of the RC element parameters can be observed, which may be provoked by structural changes due to aging (e.g. growth of SEI) with an influence on the overall impedance response and dynamic behavior of the cell and thus an influence on the impedance fitting algorithm and parameter.

3.3. Filter initialization

The most crucial leverage on the filter behavior lies in a correct filter initialization of both filters. Besides the initial starting points x_0 and θ_0 and state estimate error covariances P_0 and S_0, which quickly converge during run-time and are initially set by the maximum possible difference to the reference value, interpreted as a 1-σ-bound, particularly the noise covariances Q^x, R^x, Q^θ, R^θ strongly affect the filter response, since they are often kept constant to ensure the rigorous real-time requirement of a BMS. They enable the DEKF to include a great deal of uncertainty to cover incorrect starting values, measurement noise or errors and model inaccuracies.

As stated in Table 1, different approaches to determine those covariances have been pursued in the past. While some authors do not specify their covariances and the determination methods involved, others tune the filter covariances until the filter reaches the desired behavior. Some authors try to determine the covariances through sensor measurements. All methods have in common that they do not fully cover all model inaccuracies. An arbitrary tuning of the noise covariances may over- or underestimate the measurement, which—in the latter and worst case—turns the filter estimate to an open-loop prediction by minimizing the Kalman gain K_k. In addition, the optimality of the solution is not guaranteed. The promising way of measuring the impact of sensor noise to the model neglects the mismatch between the model and the battery. Furthermore, this method cannot be performed for the parameter estimator EKF$^\theta$, since the noise and the corresponding noise covariances Q^θ and R^θ are not physically interpretable.

We pursue a different approach, since the aforementioned methods do not really satisfy our needs. To avoid manual tuning, achieve an optimal solution and perform a method close to practice, we utilize a global gradient-free numerical optimization. The filter is set up within the MIL environment with a particular load scenario representing a standardized use-case – here, the high dynamics scenario. During run-time of the MIL environment, the reference value from the battery model is used to calculate the root-mean-square error (RMSE) to the filter estimate for both filters. To reduce an unintended and unbounded rise of the covariances, we force the filter to increase its confidence after the end of the cycle by comparing the state and parameter covariance at the start and end of the simulation and by adding an error term e if the state or parameter covariance increases. If more than one state or parameter is estimated, each corresponding diagonal entry is observed and penalized. In sum, we achieve the general objective function of the optimizer according to

$$J(\hat{x}, x, \hat{\theta}, \theta) := \begin{cases} \text{RMSE}, & \text{if } P_n < P_0 \text{ and } S_n < S_0 \ \forall\, k \in \{0, 1, \ldots, n\}, \\ \text{RMSE} + e, & \text{else} \end{cases} \tag{11}$$

where only the diagonal elements of the covariances P and S are evaluated.

The complexity of the optimization problem is high since the cost function depends nonlinearly and indirectly on search variables (covariances initialization). Therefore, we first disable the parameter estimator EKF$^\theta$ and solely optimize the short-time varying state estimator EKF^x. Only principal diagonal elements are optimized, thus allowing for easy enforcement of the positive definiteness constraint. To achieve an upfront highly stable convergence behavior of the SOC estimator that is not driven by high parameter errors, we employ the initially determined rated capacity and internal resistance. In addition to the aforementioned error term, we use an additional error term to avoid noisy behavior, i.e. high-frequency signal components. In the subsequent step, we enable the parameter estimation and set the previously determined state estimator noise covariances to constants. To avoid high influence of the state estimator, the initial value x_0 is set to the true reference. Once again, we only optimize the diagonal elements of the covariance matrix. Here, the estimation is mainly driven by the initially wrongly estimated parameters R_0 and C_p. The result of the overall

Table 2
Used fixed filter initialization parameters for the DEKF with state covariances P_0 and S_0 determined by the maximum possible deviation from the true value and noise covariances R^x, R^θ, Q^x and Q^θ obtained through numerical optimization.

State estimation		
Symbol	Parameter	Value
x_0	Initial guess	$[0.80 \;\; 0 \;\; 0]^T$
P_0	State estimate covariance	$\begin{bmatrix} 0.64 & 0 & 0 \\ 0 & 0.063 & 0 \\ 0 & 0 & 0.063 \end{bmatrix}$
R^x	Measurement noise covariance	0.77
Q^x	Process noise covariance	$\begin{bmatrix} 1.23 \times 10^{-9} & 0 & 0 \\ 0 & 5.32 \times 10^{-11} & 0 \\ 0 & 0 & 1.72 \times 10^{-4} \end{bmatrix}$
Parameter estimation		
Symbol	Parameter	Value
θ_0	Initial guess	$[3.40 \;\; 0.15]^T$
S_0	Parameter estimate covariance	$\begin{bmatrix} 11.56 & 0 \\ 0 & 0.0225 \end{bmatrix}$
R^θ	Measurement noise covariance	7.27×10^{-4}
Q^θ	Process noise covariance	$\begin{bmatrix} 1.69 \times 10^{-15} & 0 \\ 0 & 5.67 \times 10^{-11} \end{bmatrix}$

optimization process with the implemented initial datasets for the use-case study are stated in Table 2.

3.4. Chances and limitations of the approach

Due to the use of a MIL environment instead of experiments, opportunities are enabled and premises are taken that should be kept in mind in the following sections.

The use of a battery model instead of a real battery allows for easy and fast simulative assessment of various battery SOH stages and load scenarios without the effort of intensive and laborious performance of experiments. However, it ignores model inaccuracies that are induced since a model cannot completely reproduce the plant behavior and occurring parameter imbalances between parallel connected cells, as reported in [72]. Thus a SOH of 100% depicts an ideal scenario for the filter in the MIL environment, since modeling inaccuracies between the simulated battery and the filter battery model do not occur. Here, inaccuracies are introduced by modelled sensor errors only. In addition, the impact of temperature induces an additional inaccuracy that is not covered in this analysis, which is performed at 20 °C without a thermal cell model. Also, a variation in the SOC–OCV-correlation due to aging and temperature, as reported in [73], is not considered, because the focus was set to the strongly varying parameters of the cell model only. This also affects the filter initialization approach, which is only driven by a wrong starting value x_0 and θ_0. Consequently, model fitting errors do not affect the filter behavior, and the DEKF performance under degradation is highlighted solely. It should be noted that the results will certainly slightly differ if a real battery with model inaccuracies and temperature varying parameter is employed. However, the results of this analysis shall be seen as a simulative attempt to investigate the DEKF reliability under degradation and applied conditions, before this analysis is transferred to experiments, which justifies the underlying approach.

4. Results and discussion

In this analysis, the SOC and SOH determination of the DEKF under different stages of degradation and different dynamics is of special interest. First, results of the state estimation over the applied use-cases and degradation are introduced. A closer focus is given on the SOC estimation performance comparison between the simple EKF and the DEKF. Second, also parameter estimates of the DEKF are provided and analyzed according to the estimations' reliability over battery degradation. Here, capacity and internal resistance are discussed as important quantities for downstream calculations, such as SOH.

4.1. SOC estimation

The holistic assessment of the DEKF performance leads to various estimation curves for each load scenario and each degradation condition. For the sake of simplicity and to give a broad overview, the SOC estimation accuracy of the EKF and the DEKF must be transferred to a common scalar measure. The overall results are therefore summarized in a single evaluation criteria, namely the RMSE of the SOC estimation to the SOC reference in a given load scenario. The corresponding results are given in Fig. 7. Here, the DEKF SOC estimation performance is compared to the EKF SOC estimation performance in RMSE. From this graphic, several observations can be made as stated hereinafter.

Starting at the initially optimized scenario at a SOH of 100% and high dynamics, it can be seen that the DEKF structure only marginally affects the SOC estimation performance. Here, the error slightly increases by 0.1% RMSE. The maximum error can be observed during low dynamics, which is where the estimation accuracy decreases about 0.5% RMSE compared to the EKF. While the battery parameter decays, the DEKF SOC estimation performance recovers and outperforms the EKF. In general, the DEKF improves the SOC estimation accuracy in a close neighborhood of the commonly defined EOL criterion at 85% SOH starting from a 1.3% minimum up to a 1.8% maximum RMSE. If the degradation continues and reaches points far beyond the EOL at 80%, the DEKF estimation accuracy is improved to a great extent up to 8.4% compared to the simple EKF during the low and high-dynamic scenario. A general and overall trend of accuracy improvement under constant and high dynamics can be observed. The DEKF shows the best overall accuracy improvement in the high dynamics scenario. The reason for this can be found in the fact that this scenario has been used for numerical noise covariance optimization. Thus, as expected, noise

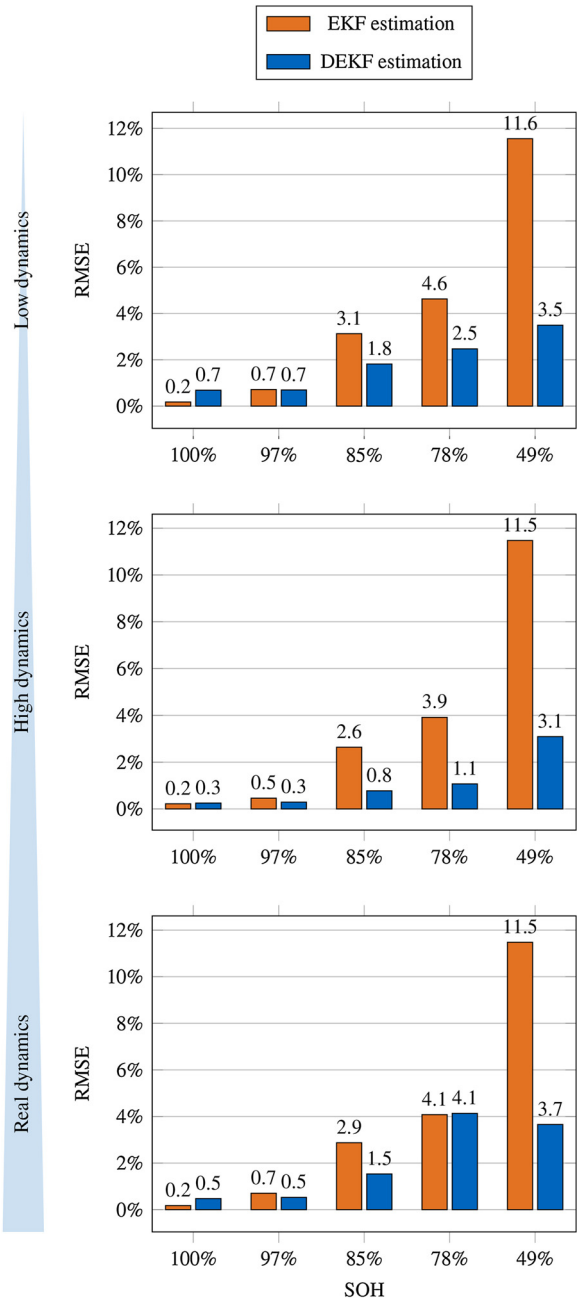

Fig. 7. Overview of the accuracy of the EKF and DEKF SOC estimation over different load dynamics and battery degradation.

covariances have a significant leverage on the estimation results and should be also determined with care involving representative load dynamics of the application. However, the DEKF struggles under the real dynamic scenario with slightly worse performance than the EKF at a SOH of 78%. Under the assumption that all three dynamic scenarios could occur in a vehicular application, the reliability of the DEKF accuracy improvement cannot be proven. In particular, this is because further inaccuracies are neglected within this analysis such as temperature influences or a model error, which additionally drive inaccuracies in the model and may further reduce the performance of the DEKF. Especially SOC estimation under close-to-realistic conditions (realistic dynamics and degradation) seems to be a challenging task for the DEKF filter algorithm.

The aforementioned results point out that the DEKF struggles with the realistic scenario under advanced battery aging in particular, since the trend of a general SOC estimation accuracy improvement cannot be obtained. Consequently, the realistic scenario should be highlighted in this analysis. In Fig. 8, the SOC reference value and both the EKF and the DEKF estimation are given for the realistic scenario over battery degradation. In addition, the absolute error $|\delta|$ between the estimates and the reference is provided with a commonly specified estimation error bound of 2% for real-world applications. As expected, if the model describes the battery cell almost perfectly and the “measurements” are only corrupted by modelled noise and quantization errors at a SOH of 100%, the EKF estimation accuracy is very high and far below 1%. We also see, that the DEKF shows a comparable but slightly weaker performance to the EKF due to the added degree of freedom of the parameter estimation and thus adding additionally interfering noise to the estimation. If battery degradation continues, the EKF estimate recovers from its incorrect starting value of 80% in the first phase but steadily drifts away. This leads to large errors under advanced degradation beyond the incorrect starting value error of 20% and may self-enforce if the last value is used as a new starting value in continuous operation, which was not within the scope of this study. A simple explanation can be found in the noise covariance determination method involved: noise covariances were determined without taking model errors due to degradation into account. If degradation occurs, noise covariances are too small to map the increasing model error and the estimate drifts away. The DEKF proves to be a good countermeasure, because the estimate quickly converges to the reference at a high SOC and steadily finds its way back to a close neighborhood of the reference value. However, at the aforementioned crucial stage of 78% SOH, the DEKF estimation shows a reinforced oscillation around the reference resulting in a larger overall error compared to the EKF estimate. Despite the fact that the DEKF SOC estimation quickly converges to the reference in the first phase and also later on if the error increases, differences partly reach unacceptable errors close to 10% far beyond the specified 2% error bound, e.g. at a SOC of approximately 40%. Surprisingly, if battery degradation increases further, the DEKF estimation visibly recovers in the crucial low SOC neighborhood and shows a better overall performance.

4.2. SOH estimation

The aforementioned erroneous observations are mainly initiated by an unsteady parameter estimation, which has a significant impact on the SOC estimation but also on the downstream SOH calculation. To assess the performance on both parameters separately, we first highlight the ohmic resistance estimation R_0 and in a subsequent step, the capacity estimation of the parameter C_p. It is worth noting that both parameters were estimated concurrently with the DEKF. The results of the ohmic resistance and capacity estimation over all use-case scenarios and all SOH stages is presented in Figs. 9 and 10, respectively.

4.2.1. Resistance estimation

Focusing on the optimization scenario in Fig. 9b, i.e. the high-dynamic scenario at an SOH of 100%, a fast convergence to the reference value can be seen. Starting at an initially estimated value of 150 mΩ, the estimation quickly approaches the reference value around 80 mΩ. Note that R_0 involves the contact resistance of the battery and is therefore superimposed by an offset, which remains constant in the MIL simulation. Over the whole simulation time, the estimation can follow the reference value, even for low SOC values at the end of the simulation time when the ohmic resistance starts to rise as depicted in k). The optimization-based initialization method enables a fast and straightforward covariance determination procedure. This behavior can also be seen for the realistic dynamical scenario in c). However, if low and temporarily constant dynamics are applied as shown in a), the previously observed accuracy cannot be maintained. Although the estimation quickly approaches a close neighborhood of the reference value in the first phase, the estimation frequently drifts away during the

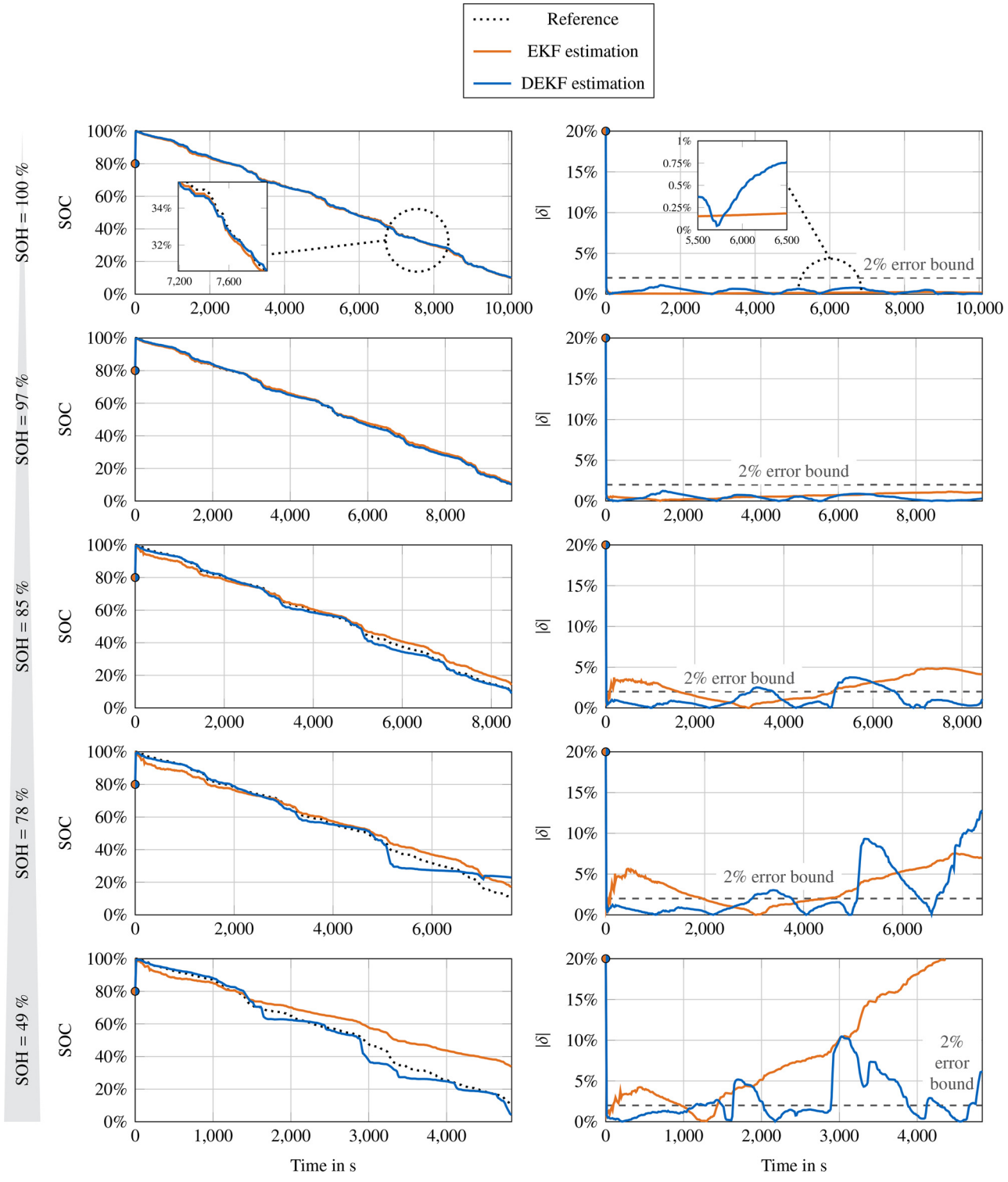

Fig. 8. Comparison of the EKF and DEKF SOC estimation performance to the SOC reference under realistic dynamics and battery degradation: true and estimated values over simulation time and battery degradation from top to bottom on the left, corresponding absolute estimation error δ to the reference on the right.

simulation. Since a constant-load scenario that discharges the battery until 10% SOC is applied, it can be concluded that the quick but only short approach of the estimation to the reference is induced by the short dynamic part of the use-case scenario. In load plateaus, the estimation tends to quickly drift away. However, if no dynamic is induced, the parameter seems to be not observable. In these cases, downstream functions such as an available power or range estimation could provide erroneous feedback and affect the longitudinal dynamics of the vehicle. It seems that the resistance estimation is only linked if a current gradient is present.

Under proceeding degradation, this erroneous behavior can be further observed. For the dynamic scenarios, however, the estimation performance is still high but involves a growing error to the reference value. Despite the fact that a lower SOH is associated with a growth of the ohmic resistance R_0 and thus a reduced gap between the initial false estimate and the true value, the DEKF struggles and cannot keep its

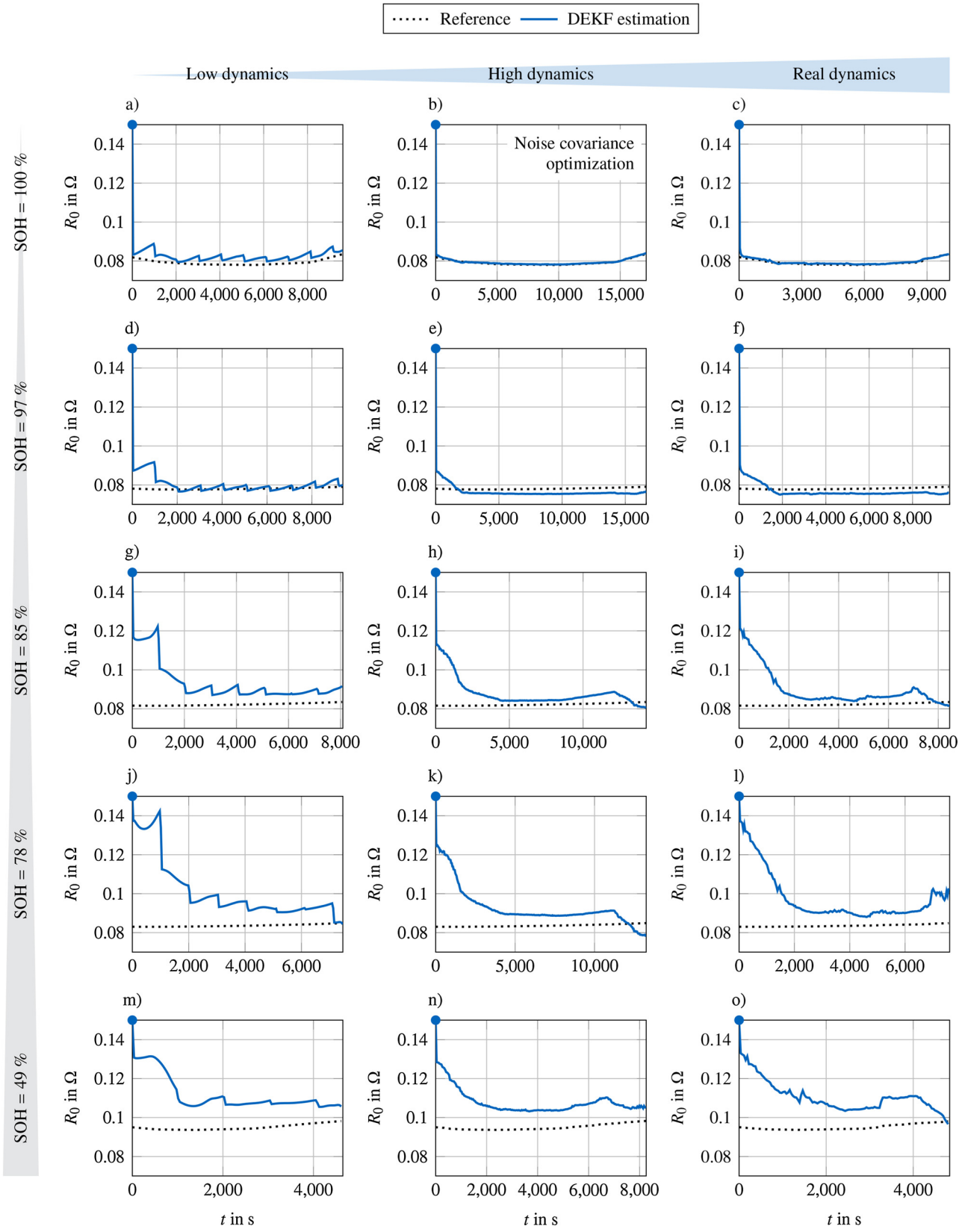

Fig. 9. Impact of battery degradation and use case scenarios on the DEKF estimation performance: R_0 estimation with increasing dynamics from left to right and fading SOH from top to bottom.

accuracy. This behavior only slightly affects the accuracy within the automotive operating range until the EOL, but could certainly affect later SOH stages under extended operation or other applications, which is exemplarily illustrated at a SOH at 49% in o).

However, it can be seen that if no precise information about the ohmic resistance is initially or operationally available, the DEKF

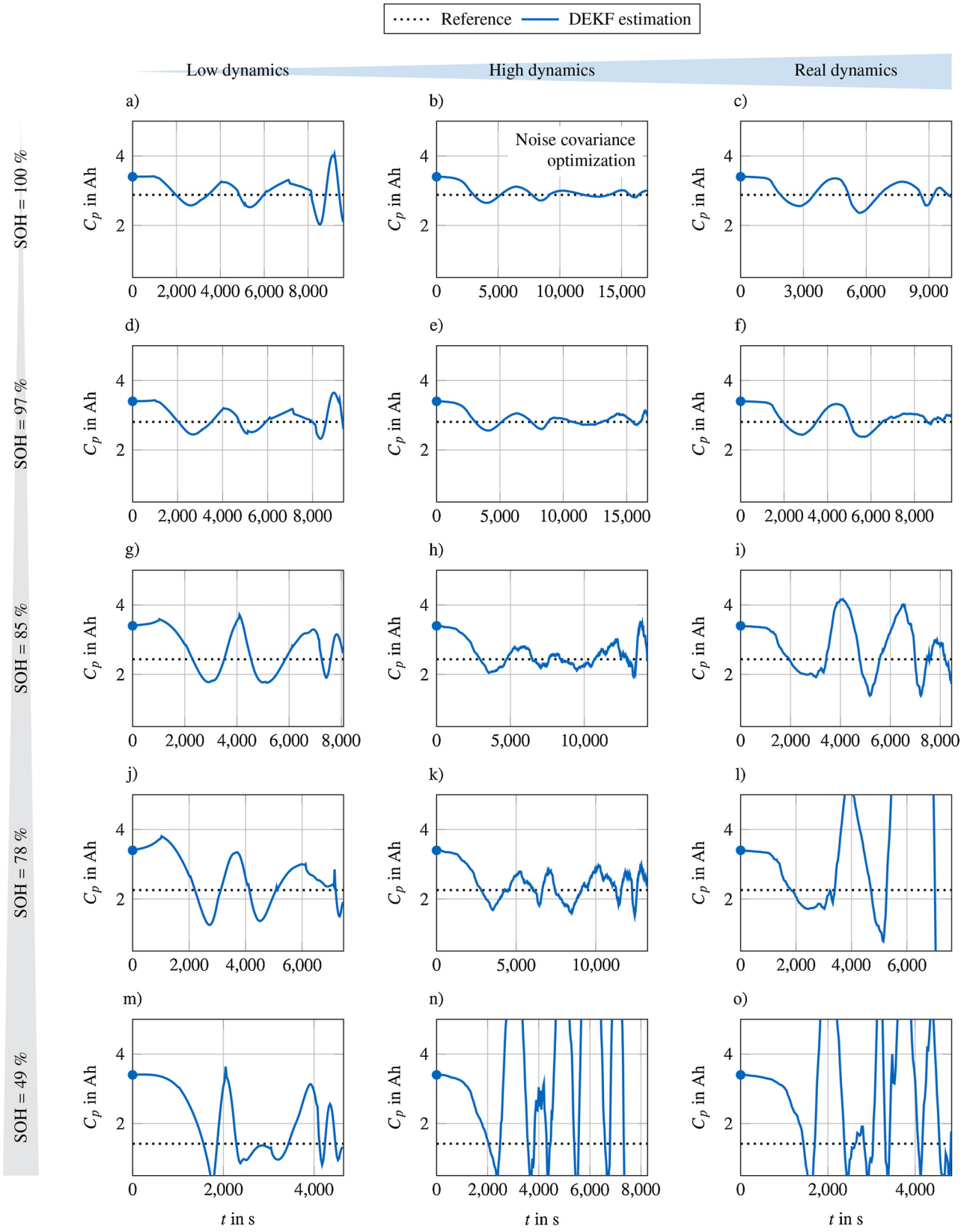

Fig. 10. Impact of battery degradation and use-case scenarios on the DEKF estimation performance: C_p estimation with increasing dynamics from left to right and fading SOH from top to bottom.

achieves promising estimation results under high dynamic load. Only under constant load, which not only occurs during constant driving resistances, but also under CC charging, the estimation has to be held or postprocessed to maintain a reliable estimation performance of the SOH and the SOC.

4.2.2. Capacity estimation

For the capacity estimation of parameter C_p, the results are less promising. Already in the initialization scenario in Fig. 10b, which is where the covariance terms are optimized to the most accurate estimation behavior, it can be seen that the estimation seems to be inert in the first phase. Later on, the estimation value oscillates around the reference, which proves that noise covariances are properly adjusted and the estimate reacts to the growing error between model and measurement. Thereby, the SOC estimation can be improved, but with a declining ability to get a precise SOH estimate. Without further postprocessing, the signal could lead to erroneous SOH estimations, depending on the sample point. Also, with direct usage of the value in downstream calculations such as state-of-power or range estimation, where the capacity parameter is necessarily needed, unstable estimation behavior would occur.

The observed unreliable behavior can also be expanded to other load dynamics. Especially in low SOC areas under constant load as shown in a), a convergence of the filter, that is a descending error between the estimate and the true reference, cannot be shown. A divergence of the estimated parameters will inevitably lead to physical misinterpretations. Based on the observations and taking into account the previously discussed SOC estimation performance, it can be concluded that, even for a perfectly fitting filter model, the capacity operates as a correction buffer for the SOC estimation, but loses its ability to represent a physical meaning. Consequently, a great challenge arises if range estimation or power prediction features should be derived.

At later SOH stages of the simulated battery life, the oscillations become intense with increasing amplitudes, as shown in n) or o). Especially at the latest stage at a SOH of 49% and realistic dynamics, the estimation totally diverges, which also influences the SOC estimation. However, until a SOH of 78% in k), the estimation reacts to the reference value despite the loss of physical meaning. Generally, DEKF struggles to estimate the capacity under advanced degradation, irrespective, whether low, high, or realistic dynamics are applied.

5. Summary, conclusions and recommendations

The main goal of this study was to evaluate the reliability of using a DEKF under a static and application-oriented initialization in order to estimate both the SOC and SOH over the battery lifetime. Three different load dynamics and five different SOH stages were used, gathered by a vehicle simulation of a validated BEV model and accelerated aging experiments, respectively.

For a reliable state and parameter estimation based on the DEKF algorithm in real-world applications, several conclusions can be drawn:

(1) If the EKF is applied only, a robust SOC estimation cannot be performed under advanced degradation given the existence of a static initialization of model parameters and noise covariances. A parameter estimating method such as DEKF is necessary to improve model accuracy and thus filter robustness, especially at late aging stages.
(2) Numerical optimization in a MIL environment is a simple and effective measure to determine optimally tuned noise covariances of the DEKF.
(3) SOC estimation can be improved generally by the DEKF compared to the simple EKF, since additional degrees of freedom enable the filter to compensate for too low noise covariances of the state estimation.
(4) Capacity estimation is strongly affected by the induced model error due to battery degradation under a given static initialization. The estimate generally oscillates around the reference, with high amplitudes under advanced degradation, especially beyond a SOH of 80%. Performed simulations provide evidence that the capacity is weakly observable. For a physical interpretation of the parameter in a downstream determination of e.g. SOH, either a further modification/extension of the algorithm or a combination with other methods is necessary to improve capacity estimation stability and thus reliability.
(5) Internal resistance estimation can be done effectively under dynamic load scenarios under a given static initialization. If dynamics are high, a close neighborhood of the true reference can be estimated. However, constant dynamics have a significant negative influence on the resistance estimation. The parameter seems to be unobservable in the aforementioned condition. Drifting estimates under constant dynamics should be countermeasured in online operation.

In a future holistical analysis of the DEKF and its modifications/extensions, model inaccuracies induced by temperature-varying parameters, choice of the model parameter identification technique and diverging cells within parallel connected cells should be considered under realistic conditions by applying the algorithm in vehicle operation.

Authors' contributions

N.W. was mainly responsible for developing, performing and writing the presented study. J.A. initiated the research on longterm stability of SOC/SOH estimation for this paper and contributed conclusions and recommendations based on the analysis results. A.F. and M.P. contributed and wrote the theoretical analysis of observability. J.A., M.P., A.F., C.R., M.L. and B.L. reviewed the manuscript. M.L. and B.L. made this work possible, gave final approval of the version to be published and agree to all aspects of the work. As a guarantor, M.L. accepts responsibility for the overall integrity of the paper.

Acknowledgements

We would like to thank the Bavarian Research Foundation for financially supporting this contribution within the project "Nutzerorientierte Elektromobilität". We are especially grateful to our colleagues Michael Baumann and Leo Wildfeuer for performing the battery aging experiments and providing the employed battery degradation dataset. Also, we would like to thank Christian Hildenbrand for his thoughtful advice.

References

[1] C.M. Martinez, X. Hu, D. Cao, E. Velenis, B. Gao, M. Wellers, Energy management in plug-in hybrid electric vehicles: recent progress and a connected vehicles perspective, IEEE Trans. Veh. Technol. 66 (6) (2017) 4534–4549, https://doi.org/10.1109/TVT.2016.2582721.
[2] S. Knupfer, R. Hensley, P. Hertzke, P. Schaufuss, N. Laverty, N. Kramer, Electrifying insights: how automakers can drive electrified vehicle sales and profitability.
[3] Y. Wang, C. Zhang, Z. Chen, A method for joint estimation of state-of-charge and available energy of LiFePO4 batteries, Appl. Energy 135 (2014) 81–87, https://doi.org/10.1016/j.apenergy.2014.08.081.
[4] V. Marano, S. Onori, Y. Guezennec, G. Rizzoni, N. Madella, Lithium-ion batteries life estimation for plug-in hybrid electric vehicles, 2009 IEEE Vehicle Power and Propulsion Conference, IEEE (2009) 536–543, https://doi.org/10.1109/VPPC.2009.5289803.
[5] W. Waag, C. Fleischer, D.U. Sauer, Critical review of the methods for monitoring of lithium-ion batteries in electric and hybrid vehicles, J. Power Sources 258 (2014) 321–339, https://doi.org/10.1016/j.jpowsour.2014.02.064.
[6] L. Lu, X. Han, J. Li, J. Hua, M. Ouyang, A review on the key issues for lithium-ion battery management in electric vehicles, J. Power Sources 226 (2013) 272–288, https://doi.org/10.1016/j.jpowsour.2012.10.060.
[7] S. Piller, M. Perrin, A. Jossen, Methods for state-of-charge determination and their applications, J. Power Sources 96 (1) (2001) 113–120, https://doi.org/10.1016/S0378-7753(01)00560-2.

[8] K. Propp, D.J. Auger, A. Fotouhi, S. Longo, V. Knap, Kalman-variant estimators for state of charge in lithium-sulfur batteries, J. Power Sources 343 (2017) 254–267, https://doi.org/10.1016/j.jpowsour.2016.12.087.

[9] M. Broussely, P. Biensan, F. Bonhomme, P. Blanchard, S. Herreyre, K. Nechev, R.J. Staniewicz, Main aging mechanisms in Li-ion batteries, J. Power Sources 146 (1-2) (2005) 90–96, https://doi.org/10.1016/j.jpowsour.2005.03.172.

[10] J. Vetter, P. Novák, M.R. Wagner, C. Veit, K.-C. Möller, J.O. Besenhard, M. Winter, M. Wohlfahrt-Mehrens, C. Vogler, A. Hammouche, Ageing mechanisms in lithium-ion batteries, J. Power Sources 147 (1-2) (2005) 269–281, https://doi.org/10.1016/j.jpowsour.2005.01.006.

[11] M. Berecibar, I. Gandiaga, I. Villarreal, N. Omar, J. van Mierlo, P. van den Bossche, Critical review of state of health estimation methods of Li-ion batteries for real applications, Renew. Sustain. Energy Rev. 56 (2016) 572–587, https://doi.org/10.1016/j.rser.2015.11.042.

[12] C.R. Birkl, M.R. Roberts, E. McTurk, P.G. Bruce, D.A. Howey, Degradation diagnostics for lithium ion cells, J. Power Sources 341 (2017) 373–386, https://doi.org/10.1016/j.jpowsour.2016.12.011.

[13] A. Maheshwari, M. Heck, M. Santarelli, Cycle aging studies of lithium nickel manganese cobalt oxide-based batteries using electrochemical impedance spectroscopy, Electrochim. Acta 273 (2018) 335–348, https://doi.org/10.1016/j.electacta.2018.04.045.

[14] J. Schmitt, A. Maheshwari, M. Heck, S. Lux, M. Vetter, Impedance change and capacity fade of lithium nickel manganese cobalt oxide-based batteries during calendar aging, J. Power Sources 353 (2017) 183–194, https://doi.org/10.1016/j.jpowsour.2017.03.090.

[15] P. Singh, R. Vinjamuri, X. Wang, D. Reisner, Design and implementation of a fuzzy logic-based state-of-charge meter for Li-ion batteries used in portable defibrillators, J. Power Sources 162 (2) (2006) 829–836, https://doi.org/10.1016/j.jpowsour.2005.04.039.

[16] X. Hu, S.E. Li, Y. Yang, Advanced machine learning approach for lithium-ion battery state estimation in electric vehicles, IEEE Trans. Transp. Electr. 2 (2) (2016) 140–149, https://doi.org/10.1109/TTE.2015.2512237.

[17] T. Hansen, C.-J. Wang, Support vector based battery state of charge estimator, J. Power Sources 141 (2) (2005) 351–358, https://doi.org/10.1016/j.jpowsour.2004.09.020.

[18] G.L. Plett, Extended Kalman filtering for battery management systems of LiPB-based hev battery packs: Part 1, J. Power Sources 134 (2) (2004) 252–261, https://doi.org/10.1016/j.jpowsour.2004.02.031.

[19] G.L. Plett, Extended Kalman filtering for battery management systems of LiPB-based hev battery packs: Part 2, J. Power Sources 134 (2) (2004) 262–276, https://doi.org/10.1016/j.jpowsour.2004.02.032.

[20] G.L. Plett, Extended Kalman filtering for battery management systems of LiPB-based hev battery packs: Part 3, J. Power Sources 134 (2) (2004) 277–292, https://doi.org/10.1016/j.jpowsour.2004.02.033.

[21] Z. Chen, Y. Fu, C.C. Mi, State of charge estimation of lithium-ion batteries in electric drive vehicles using extended Kalman filtering, IEEE Trans. Veh. Technol. 62 (3) (2013) 1020–1030, https://doi.org/10.1109/TVT.2012.2235474.

[22] J. Li, J. Klee Barillas, C. Guenther, M.A. Danzer, A comparative study of state of charge estimation algorithms for LiFePO4 batteries used in electric vehicles, J. Power Sources 230 (2013) 244–250, https://doi.org/10.1016/j.jpowsour.2012.12.057.

[23] G.L. Plett, Sigma-point Kalman filtering for battery management systems of LiPB-based hev battery packs, J. Power Sources 161 (2) (2006) 1369–1384, https://doi.org/10.1016/j.jpowsour.2006.06.004.

[24] G.L. Plett, Sigma-point Kalman filtering for battery management systems of LiPB-based hev battery packs, J. Power Sources 161 (2) (2006) 1356–1368, https://doi.org/10.1016/j.jpowsour.2006.06.003.

[25] F. Sun, X. Hu, Y. Zou, S. Li, Adaptive unscented Kalman filtering for state of charge estimation of a lithium-ion battery for electric vehicles, Energy 36 (5) (2011) 3531–3540, https://doi.org/10.1016/j.energy.2011.03.059.

[26] W. He, N. Williard, C. Chen, M. Pecht, State of charge estimation for electric vehicle batteries using unscented Kalman filtering, Microelectron. Reliab. 53 (6) (2013) 840–847, https://doi.org/10.1016/j.microrel.2012.11.010.

[27] Y. Tian, B. Xia, W. Sun, Z. Xu, W. Zheng, A modified model based state of charge estimation of power lithium-ion batteries using unscented Kalman filter, J. Power Sources 270 (2014) 619–626, https://doi.org/10.1016/j.jpowsour.2014.07.143.

[28] L. Zhong, C. Zhang, Y. He, Z. Chen, A method for the estimation of the battery pack state of charge based on in-pack cells uniformity analysis, Appl. Energy 113 (2014) 558–564, https://doi.org/10.1016/j.apenergy.2013.08.008.

[29] X. Liu, Z. Chen, C. Zhang, J. Wu, A novel temperature-compensated model for power li-ion batteries with dual-particle-filter state of charge estimation, Appl. Energy 123 (2014) 263–272, https://doi.org/10.1016/j.apenergy.2014.02.072.

[30] W. Wang, D. Wang, X. Wang, T. Li, R. Ahmed, S. Habibi, A. Emadi, Comparison of Kalman filter-based state of charge estimation strategies for Li-Ion batteries, 2016 IEEE Transportation Electrification Conference and Expo (ITEC), IEEE (2016) 1–6, https://doi.org/10.1109/ITEC.2016.7520302.

[31] X. Hu, D. Cao, B. Egardt, Condition monitoring in advanced battery management systems: Moving horizon estimation using a reduced electrochemical model, IEEE/ASME Trans. Mechatron. 23 (1) (2018) 167–178, https://doi.org/10.1109/TMECH.2017.2675920.

[32] I.-S. Kim, Nonlinear state of charge estimator for hybrid electric vehicle battery, IEEE Trans. Power Electron. 23 (4) (2008) 2027–2034, https://doi.org/10.1109/TPEL.2008.924629.

[33] S.J. Moura, N.A. Chaturvedi, M. Krstic, Pde estimation techniques for advanced battery management systems – Part I: SOC estimation, 2012 American Control Conference (ACC), IEEE (2012) 559–565, https://doi.org/10.1109/ACC.2012.6315019.

[34] F. Zhang, G. Liu, L. Fang, H. Wang, Estimation of battery state of charge with h-infinity observer: applied to a robot for inspecting power transmission lines, IEEE Trans. Ind. Electron. 59 (2) (2012) 1086–1095, https://doi.org/10.1109/TIE.2011.2159691.

[35] Y. Wang, H. Fang, Z. Sahinoglu, T. Wada, S. Hara, Adaptive estimation of the state of charge for lithium-ion batteries: nonlinear geometric observer approach, IEEE Trans. Control Syst. Technol. 23 (3) (2015) 948–962, https://doi.org/10.1109/TCST.2014.2356503.

[36] S. Dey, B. Ayalew, P. Pisu, Nonlinear robust observers for state-of-charge estimation of lithium-ion cells based on a reduced electrochemical model, IEEE Trans. Control Syst. Technol. 23 (5) (2015) 1935–1942, https://doi.org/10.1109/TCST.2014.2382635.

[37] Y. Zou, X. Hu, H. Ma, S.E. Li, Combined state of charge and state of health estimation over lithium-ion battery cell cycle lifespan for electric vehicles, J. Power Sources 273 (2015) 793–803, https://doi.org/10.1016/j.jpowsour.2014.09.146.

[38] D. Andre, C. Appel, T. Soczka-Guth, D.U. Sauer, Advanced mathematical methods of SOC and SOH estimation for lithium-ion batteries, J. Power Sources 224 (2013) 20–27, https://doi.org/10.1016/j.jpowsour.2012.10.001.

[39] I.-S. Kim, A technique for estimating the state of health of lithium batteries through a dual-sliding-mode observer, IEEE Trans. Power Electron. 25 (4) (2010) 1013–1022, https://doi.org/10.1109/TPEL.2009.2034966.

[40] S. Schwunk, N. Armbruster, S. Straub, J. Kehl, M. Vetter, Particle filter for state of charge and state of health estimation for lithium-iron phosphate batteries, J. Power Sources 239 (2013) 705–710, https://doi.org/10.1016/j.jpowsour.2012.10.058.

[41] M. Urbain, S. Rael, B. Davat, P. Desprez, State estimation of a lithium-ion battery through Kalman filter, 2007 IEEE Power Electronics Specialists Conference, IEEE (2007) 2804–2810, https://doi.org/10.1109/PESC.2007.4342463.

[42] S. Lee, J. Kim, J. Lee, B.H. Cho, State-of-charge and capacity estimation of lithium-ion battery using a new open-circuit voltage versus state-of-charge, J. Power Sources 185 (2) (2008) 1367–1373, https://doi.org/10.1016/j.jpowsour.2008.08.103.

[43] M. Rubagotti, S. Onori, G. Rizzoni, Automotive battery prognostics using dual extended Kalman filter, ASME 2009 Dynamic Systems and Control Conference, Volume 2, ASME (2009) 257–263, https://doi.org/10.1115/DSCC2009-2725.

[44] C. Hu, B.D. Youn, J. Chung, A multiscale framework with extended Kalman filter for lithium-ion battery SOC and capacity estimation, Appl. Energy 92 (2012) 694–704, https://doi.org/10.1016/j.apenergy.2011.08.002.

[45] J. Kim, B.H. Cho, Pattern recognition for temperature-dependent state-of-charge/capacity estimation of a Li-ion cell, IEEE Trans. Energy Convers. 28 (1) (2013) 1–11, https://doi.org/10.1109/TEC.2012.2222884.

[46] M. Mastali, J. Vazquez-Arenas, R. Fraser, M. Fowler, S. Afshar, M. Stevens, Battery state of the charge estimation using Kalman filtering, J. Power Sources 239 (2013) 294–307, https://doi.org/10.1016/j.jpowsour.2013.03.131.

[47] T. Dragicevic, S. Sucic, J.M. Guerrero, Battery state-of-charge and parameter estimation algorithm based on Kalman filter, Eurocon 2013, IEEE (2013) 1519–1525, https://doi.org/10.1109/EUROCON.2013.6625179.

[48] G. Walder, C. Campestrini, M. Lienkamp, A. Jossen, Adaptive state and parameter estimation of lithium-ion batteries based on a dual linear Kalman filter, The Second International Conference on Technological Advances in Electrical, Electronics and Computer Engineering (TAEECE2014), The Society of Digital Information and Wireless Communication (2014).

[49] R. Xiong, F. Sun, Z. Chen, H. He, A data-driven multi-scale extended Kalman filtering based parameter and state estimation approach of lithium-ion olymer battery in electric vehicles, Appl. Energy 113 (2014) 463–476, https://doi.org/10.1016/j.apenergy.2013.07.061.

[50] C. Campestrini, G. Walder, A. Jossen, M. Lienkamp, Temperature influences on state and parameter estimation based on a dual Kalman filter, Conference on Future Automotive Technology (CoFAT) (2014).

[51] C. Campestrini, T. Heil, S. Kosch, A. Jossen, A comparative study and review of different Kalman filters by applying an enhanced validation method, J. Energy Storage 8 (2016) 142–159, https://doi.org/10.1016/j.est.2016.10.004.

[52] S. Nejad, D.T. Gladwin, D.A. Stone, On-chip implementation of extended Kalman filter for adaptive battery states monitoring, Proceedings of the IECON 2016 – 42nd Annual Conference of the IEEE Industrial Electronics Society, IEEE, [Piscataway, N.J.] (2016) 5513–5518, https://doi.org/10.1109/IECON.2016.7793527.

[53] S. Li, S. Pischinger, C. He, L. Liang, M. Stapelbroek, A comparative study of model-based capacity estimation algorithms in dual estimation frameworks for lithium-ion batteries under an accelerated aging test, Appl. Energy 212 (2018) 1522–1536, https://doi.org/10.1016/j.apenergy.2018.01.008.

[54] M.A. Hannan, M. Lipu, A. Hussain, A. Mohamed, A review of lithium-ion battery state of charge estimation and management system in electric vehicle applications: Challenges and recommendations, Renew. Sustain. Energy Rev. 78 (2017) 834–854, https://doi.org/10.1016/j.rser.2017.05.001.

[55] A. Farmann, W. Waag, D.U. Sauer, Adaptive approach for on-board impedance parameters and voltage estimation of lithium-ion batteries in electric vehicles, J. Power Sources 299 (2015) 176–188, https://doi.org/10.1016/j.jpowsour.2015.08.087.

[56] S. Nejad, D.T. Gladwin, D.A. Stone, A systematic review of lumped-parameter equivalent circuit models for real-time estimation of lithium-ion battery states, J. Power Sources 316 (2016) 183–196, https://doi.org/10.1016/j.jpowsour.2016.03.042.
[57] Y. Firouz, R. Relan, J.M. Timmermans, N. Omar, P. van den Bossche, J. van Mierlo, Advanced lithium ion battery modeling and nonlinear analysis based on robust method in frequency domain: nonlinear characterization and non-parametric modeling, Energy 106 (2016) 602–617, https://doi.org/10.1016/j.energy.2016.03.028.
[58] A. Farmann, W. Waag, D.U. Sauer, Application-specific electrical characterization of high power batteries with lithium titanate anodes for electric vehicles, Energy 112 (2016) 294–306, https://doi.org/10.1016/j.energy.2016.06.088.
[59] S. Haykin, Kalman Filtering and Neural Networks, 1st Edition, Wiley series on adaptive and learning systems for signal processing, communications, and control, [s. n.], [S. l.], (2001).
[60] S. Sepasi, R. Ghorbani, B.Y. Liaw, A novel on-board state-of-charge estimation method for aged Li-ion batteries based on model adaptive extended Kalman filter, J. Power Sources 245 (2014) 337–344, https://doi.org/10.1016/j.jpowsour.2013.06.108.
[61] C. Campestrini, S. Kosch, A. Jossen, Influence of change in open circuit voltage on the state of charge estimation with an extended Kalman filter, J. Energy Storage 12 (2017) 149–156, https://doi.org/10.1016/j.est.2017.04.011.
[62] P. Shen, M. Ouyang, L. Lu, J. Li, State of charge, state of health and state of function co-estimation of lithium-ion batteries for electric vehicles, 2016 IEEE Vehicle Power and Propulsion Conference (VPPC), IEEE (2016) 1–5, https://doi.org/10.1109/VPPC.2016.7791782.
[63] J. Remmlinger, M. Buchholz, M. Meiler, P. Bernreuter, K. Dietmayer, State-of-health monitoring of lithium-ion batteries in electric vehicles by on-board internal resistance estimation, J. Power Sources 196 (12) (2011) 5357–5363, https://doi.org/10.1016/j.jpowsour.2010.08.035.
[64] J. Remmlinger, M. Buchholz, T. Soczka-Guth, K. Dietmayer, On-board state-of-health monitoring of lithium-ion batteries using linear parameter-varying models, J. Power Sources 239 (2013) 689–695, https://doi.org/10.1016/j.jpowsour.2012.11.102.
[65] C. Campestrini, M.F. Horsche, I. Zilberman, T. Heil, T. Zimmermann, A. Jossen, Validation and benchmark methods for battery management system functionalities: state of charge estimation algorithms, J. Energy Storage 7 (2016) 38–51, https://doi.org/10.1016/j.est.2016.05.007.
[66] L. Lin, M. Fukui, K. Takaba, An accurate SOC estimation system for lithium-ion batteries by EKF with dynamic noise adjustment, ISCIT 2015, IEEE, Piscataway, NJ and Piscataway, NJ (2015) 33–36, https://doi.org/10.1109/ISCIT.2015.7458300.
[67] R. Hermann, A. Krener, Nonlinear controllability and observability, IEEE Trans. Autom. Control 22 (5) (1977) 728–740, https://doi.org/10.1109/TAC.1977.1101601.
[68] J. Birk, M. Zeitz, Computer-aided analysis of nonlinear observation problems, IFAC Proc. Vol. 25 (13) (1992) 257–262, https://doi.org/10.1016/S1474-6670(17)52291-0.
[69] P. Niermeyer, M. Pak, B. Lohmann, A control effectiveness estimator with a moving horizon robustness modification for fault-tolerant hexacopter control, IFAC-PapersOnLine 50 (1) (2017) 270–275, https://doi.org/10.1016/j.ifacol.2017.08.045.
[70] S. Zhao, S.R. Duncan, D.A. Howey, Observability analysis and state estimation of lithium-ion batteries in the presence of sensor biases, IEEE Trans. Control Syst. Technol. 25 (1) (2017) 326–333, https://doi.org/10.1109/TCST.2016.2542115.
[71] J. Adermann, D. Brecheisen, P. Wacker, M. Lienkamp, Parameter estimation of traction batteries by energy and charge counting during reference cycles, Conference on Future Automotive Technology (CoFAT) (2017) 1–7.
[72] M. Baumann, L. Wildfeuer, S. Rohr, M. Lienkamp, Parameter variations within Li-Ion battery packs – theoretical investigations and experimental quantification, J. Energy Storage 18 (2018) 295–307, https://doi.org/10.1016/j.est.2018.04.031.
[73] A. Farmann, D.U. Sauer, A study on the dependency of the open-circuit voltage on temperature and actual aging state of lithium-ion batteries, J. Power Sources 347 (2017) 1–13, https://doi.org/10.1016/j.jpowsour.2017.01.098.